Selective Laser Sintering of Polycarbonate at Varying Powers, Scan Speeds and Scan Spacings

Childs T. H. C., Cardie S. and Brown J.M.,

University of Leeds, UK

Moving heat source theory has been combined with a sintering model to predict densification in the bulk of and round the edges of a sintered block. The edge effects are related to size errors in sintering. Experiments support the modelling.

INTRODUCTION

A benchmark study (1) has shown selective laser sintering to be the equal of or to have accuracy advantages over other processes for creating parts of size over 10 mm. Experience is needed to achieve best accuracies, as with other processes. This paper is (for us) a first step in understanding the relation between sintering parameters, part size and acuracy.

Work at the University of Texas at Austin (2-4) has established that the sintering of polycarbonate can be understood in terms of a rate model driven by viscous and surface tension effects. Material properties are such that a sharp boundary exists between sintered and unsintered material. When full density is not achieved in a part, density within a single layer varies from fully sintered to totally unsintered; measured part density is thus a mean of widely varying values. Published work (3-4) uses a one-dimensional non-steady state heat flow model to calculate the temperature profile and densification beneath the surface and concentrates on the effects on this of material properties varying with temperature and during sintering. In this paper, these variations are ignored but a three dimensional non-steady heat flow is used to enable edge effects to be estimated. Density gradients at edges are assumed to be responsible for variations of accuracy with sintering parameters, part size, part shape and orientation.

THEORY

The geometry studied is a rectangular block ABCD of width w and length a (figure 1a), sintered by a laser spot of diameter d and power P, travelling at speed U in the x-direction and incrementing in the y-direction by the scan spacing s. The block is made up of layers of thickness z_r (figure 1b) but, because of densification, the thickness of the powder layer being sintered, z_l, is greater than z_r. The calculation has three stages: modelling the heat source, calculating the variation of temperature with time around the heat source, and estimating the density changes caused by the temperature distribution.

Modelling the heat source. Observation of selective laser sintering shows a sintering front to move steadily in the y-direction. In this paper the actual rastering spot is simplified to a strip source of width d, emitting heat q per unit area per unit

time uniformly and moving steadily in the y-direction with speed V. V is found from the time t* to advance the distance s:

$$V = s/t^* \qquad (1)$$

where $t^* = w(1/U + 1/U_r) + t_d$ (2).

U_r is the speed of the returning scan and t_d is the sum of any laser dwell times. By equating the heat put into the block by the simplified source to that put in by the actual rastering spot it is found that q/V, needed later, is

$$q/V = (P/Us) / d \qquad (3).$$

The smearing out of the rastering spot source to a steadily moving strip source is unable to model any periodic density variations that may occur in the y-direction. It must clearly become an oversimplification as s becomes much greater than d, but in practice there is some overlap between successive scans. It is also an oversimplification if heat diffuses further than the source width d in the cycle time t*. When U and U_r are approximately the same and t_d is negligible, it can be shown that for the validity of the approximation

$$U/w \geq 2\kappa/d^2 \qquad (4),$$

where κ is the diffusivity of the material. It will be seen that this is satisfied in typical sintering situations, up to widths w around 100 mm or so.

Temperature calculation. A classical moving heat source result (5) gives the temperature rise T in a semi-infinite body $z > 0$ caused by a rectangular surface source of sides 2l (=d) parallel to y and 2b (=w) parallel to x, moving with speed V in the y direction, and that has been transmitting heat for time t, as

$$T = \frac{\alpha q}{V}\frac{\kappa/k}{2\sqrt{2\pi}}\int_0^{V^2t/2\kappa}\frac{e^{-Z^2/2u}}{\sqrt{u}}\left(\operatorname{erf}\frac{X+B}{\sqrt{2u}} - \operatorname{erf}\frac{X-B}{\sqrt{2u}}\right)\left(\operatorname{erf}\frac{Y+L+u}{\sqrt{2u}} - \operatorname{erf}\frac{Y-L+u}{\sqrt{2u}}\right)du$$

where $X = \frac{Vx}{2\kappa}$, $Y = \frac{Vy}{2\kappa}$, $Z = \frac{Vz}{2\kappa}$, $L = \frac{Vl}{2\kappa}$ and $B = \frac{Vb}{2\kappa}$ (5).

The origin of the axes x, y, z is centred in the heat source, α is the fraction of heat absorbed by the body and k is the thermal conductivity of the body.

Equation (4) has been integrated numerically to provide temperature fields relative to the position of the heat source in four special cases:(i) the steady state temperatures away from the edges of the block; (ii) the steady state temperatures around the edges AC and BD of the block; (iii) the initial temperatures around the edge AB; and (iv), by superposition of (i) less (iii), the final temperatures around the edge CD. κ and k have been taken as constant and to have values appropriate to the unsintered powder. The volume contractions due to sintering during heating have been ignored. These are on the grounds that it is the temperature distribution in the powder around the sintering front that determines the front's spatial extent. The fact that there is a previously sintered layer beneath the current powder layer (with thermal properties of the solid) has also been ignored.

Densification. The simple model of densification used in (4) has been applied:

$$-\frac{d\varepsilon}{\varepsilon} = \int_0^t Ae^{(-E/RT)}dt \qquad (6)$$

where ε is the porosity of the powder. The temperature / time history at a depth z below the surface has been used to integrate the right hand side of (6) and hence obtain the sintered density at that depth. The mean density has been obtained by averaging over the layer thickness. The contractions in z are included at this stage.

Calculations have been performed with thermal data from (4):κ = 0.1 mm^2/s, α = 0.95, k = 0.08 W/m/°K, E/R = 21,000 and A = 8.84x10^{16} s^{-1}; and for d = 0.2 mm, z_r = 0.125 mm and a powder bed ambient temperature of 154°C. Figure 2 shows predicted densities away from the part edges as a function of laser power. For w = 25 mm, density depends only on the energy density parameter P/(Us), but for larger values of w, an effect of cooling between scans is predicted. For P/(Us) = 0.045 J/mm^2, the hatched range for w = 90 mm has been obtained by varying U and s in different combinations. Figure 3 shows predicted edge density variations when w = 25 mm. In figure 3a (for the edges AC and BD) it is noticeable that sinterng occurs outside the geometric boundary. This is not the case, in figure 3b, for the edges AB and CD. For these the density profiles differ from one another as there is no heat in the layer before sintering starts, but heat must diffuse away after the sintering is completed.

EXPERIMENTATION

A standard test piece (figure 4a) was sintered. Pieces were created at positions 1 to 21 in the build zone of a Sinterstation 2000 as indicated in figure 4b. Parts were built with laser powers from 4.5 to 19 W, scan speeds from 517 to 1206 mm/s, scan spacings from 0.08 to 0.406 mm, chosen to surround the manufacturer's recommended settings for polycarbonate of 11 W, 861 mm/s and 0.203 mm. The layer thickness was 0.125 mm. All other variables were held at the manufacturer's recommended defaults. In particular the ambient temperature of the powder bed was 154°C, the nominal beam diameter was 0.2 mm.

RESULTS

In a first test all 21 parts were sintered with P= 11 W, U = 860 mm/s and s = 0.203 mm (P/Us = 0.063 J/mm^2). The slightly lower density of parts 1 to 9 (w = 90 mm) than 10 to 15 and 16 to 21 (w = 25 mm) is seen in figure 5a, but in each group there is one low value. These, from parts 12, 9 and 19, may be caused by a slightly lower bed temperature near to the edge of the build zone (by accident the pattern of parts, figure 4b, was not quite concentric in the zone). These effects combine to give a general scatter of results as shown in figure 5b. In a second test, the full range of P, U and s variables was used to study how density varied with P/Us. Figure 6 (•) is the result. Figure 6 also shows a third test result (o) in which P, U and s were varied, keeping P/Us constant, results derived from figure 26 of reference 4 (+), the theoretical prediction for w = 25 mm from figure 2 and another prediction discussed later. Finally, over- and under-size x and y measurements are presented in figure 7 with theoretical predictions obtained from figure 3 assuming that a density of 650 kg/m^3 marks the boundary of the part.

DISCUSSION AND CONCLUSION

Figure 6 (•) shows that within the scatter of results established in figure 5 density depends mainly on the energy density P/Us. A small influence of w has been found (figure 5), but less than expected from figure 2. Densities (•) are significantly less than the theory. There can be a small variability between runs (results (o) differ from (•)) and it is interesting to note the small differences between the present experimental work and that of reference (4) (+), although the layer thickness used in (4) is not clear. The overprediction of density may result from neglecting the changes in k during sintering. Repeating the calculations using solid material thermal properties gives a better agreement, as indicated in figure 6 (k = 0.2 W/m/°K). Perhaps a role of previously sintered material is to conduct heat more rapidly away from the sintering zone.

The under- and over-size measurements of figure 7 are very scattered, perhaps reflecting difficulties of measurement or variablity in breakout and cleaning techniques. Their variation with P/Us is similar to the predicted values. Figure 3 suggests different beam offsets should be used for x and y edges.

These studies are at an early stage. The results encourage further developments to create automatic techniques for controlling sintering conditions and beam offsets for required part densities and accuracies.

ACKNOWLEDGEMENT

Our purchase of a selective laser sintering machine was made possible by participation in a European project EUREKA EU776 and the generosity of the University of Leeds and its Departments of Mechanical Engineering and Applied Mathematics. The experimental studies were developed by undergraduate students J. Bailey, A. Medancos, J. Morris and G. Weaver.

REFERENCES

1. Juster N. P. and Childs T. H. C., A comparison of rapid prototyping processes, Proc. 3rd European Conf. Rapid Prototyping, pp.35-52, Nottingham 1994.
2. Barlow J. W., Sun M. S. M. and Beaman J. J., Analysis of selective laser sintering, Proc. 2nd. Int. Conf. on Rapid Prototyping (Lightman A. J. and Chartoff R. P. eds.), pp. 1-14, Dayton, Ohio 1991.
3. Zong G. et al., Laser processing in solid freeform fabrication, Int. Conf. on Beam Processing of Advanced Materials (Singh J. and Copley S. M. eds.), pp97-110, The Minerals, Metals and Materials Society 1993.
4. Nelson J. C. et al., Model of the selective laser sintering of bisphenol-A polycarbonate, Ind. Eng. Chem. Res., 1993, 32, 2305-2317.
5. Jaeger J. C., Moving sources of heat and the temperature at sliding contacts, Jnl. Roy. Soc. New South Wales, 1942, 76, 203-224.

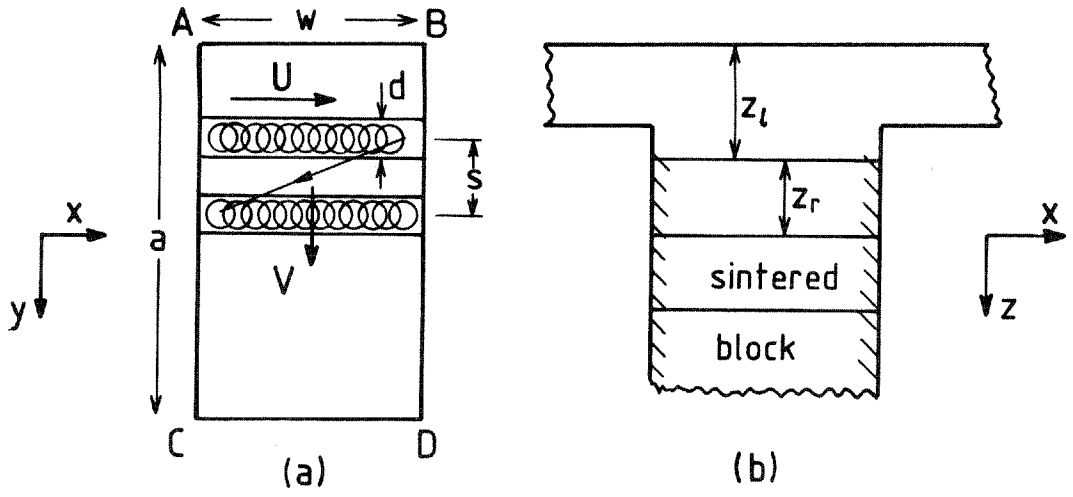

Figure 1. The sintering geometry.

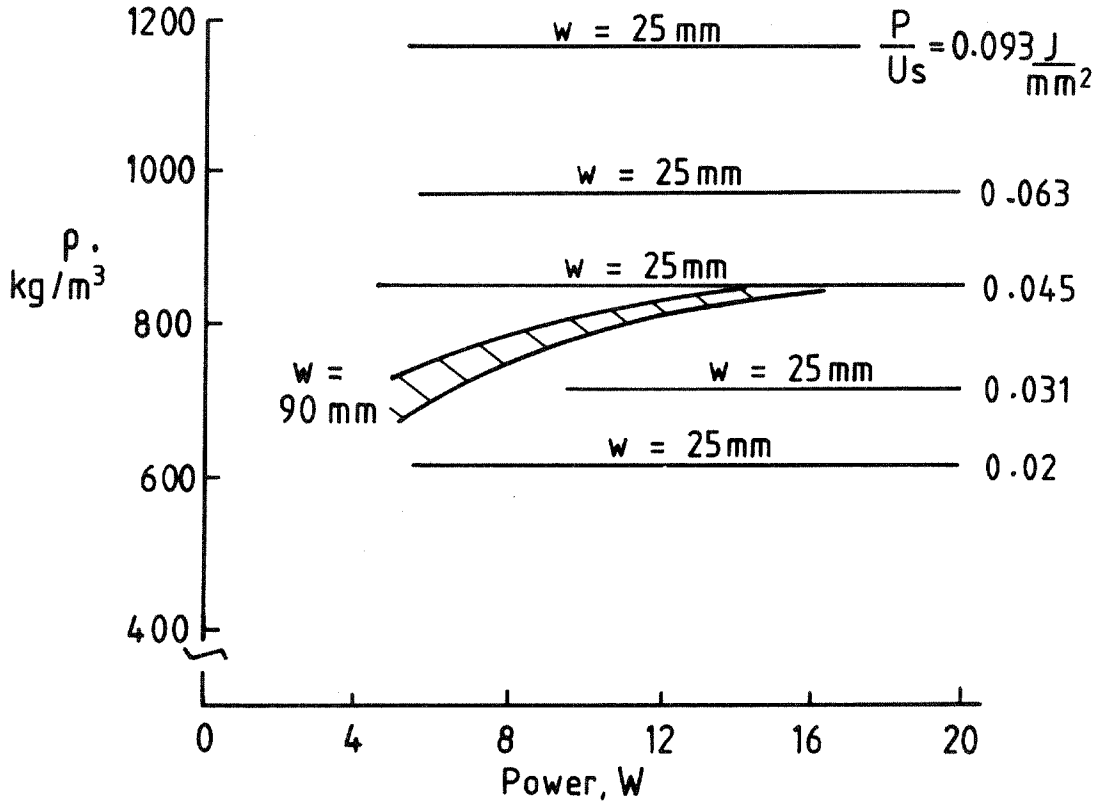

Figure 2. Dependence of density on laser power for a range of scan widths w and energy densities P/(Us).

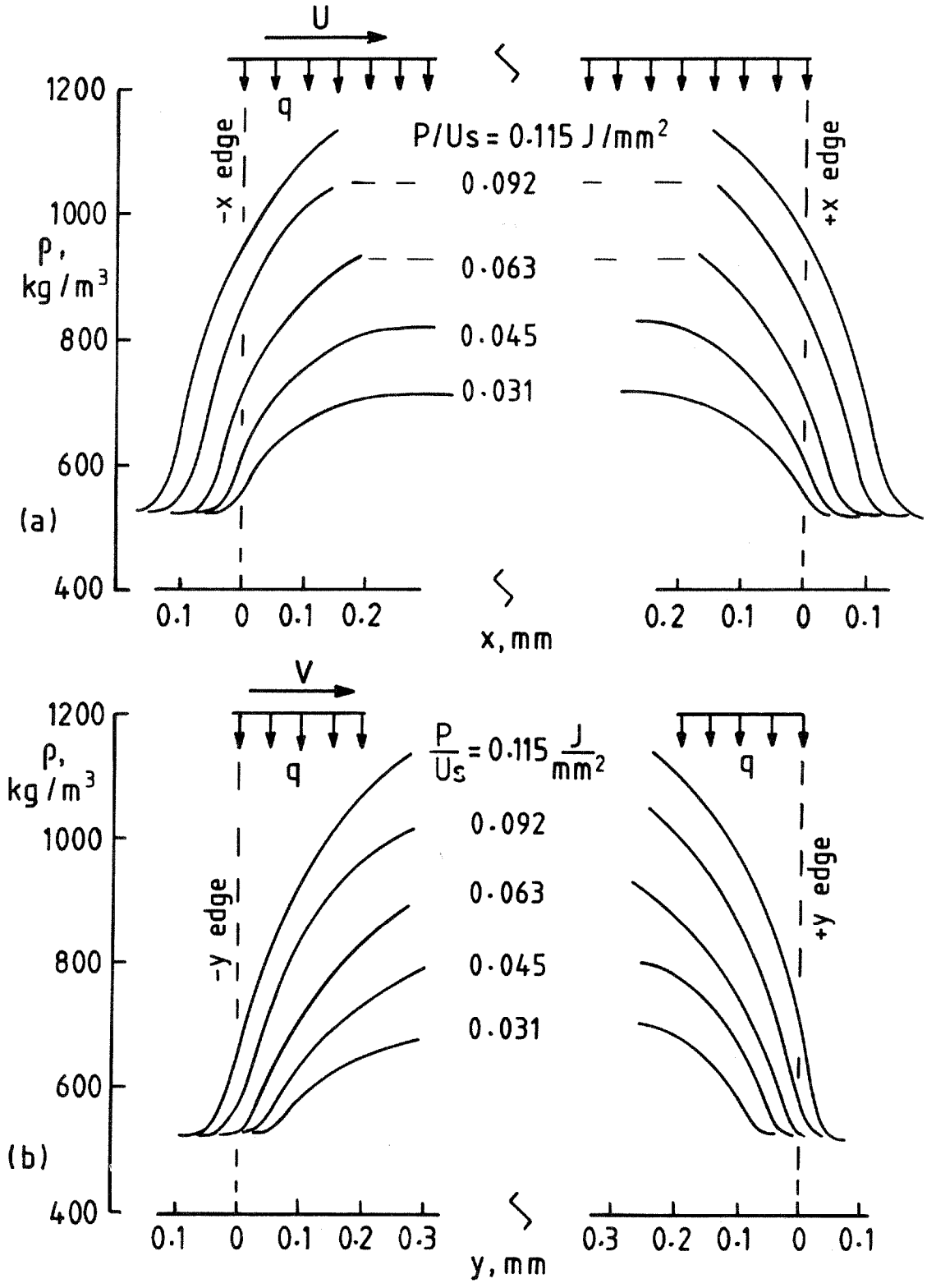

Figure 3. Density variations round the edges of a part: (a) x (side) edges; (b) start and finish (y) edges.

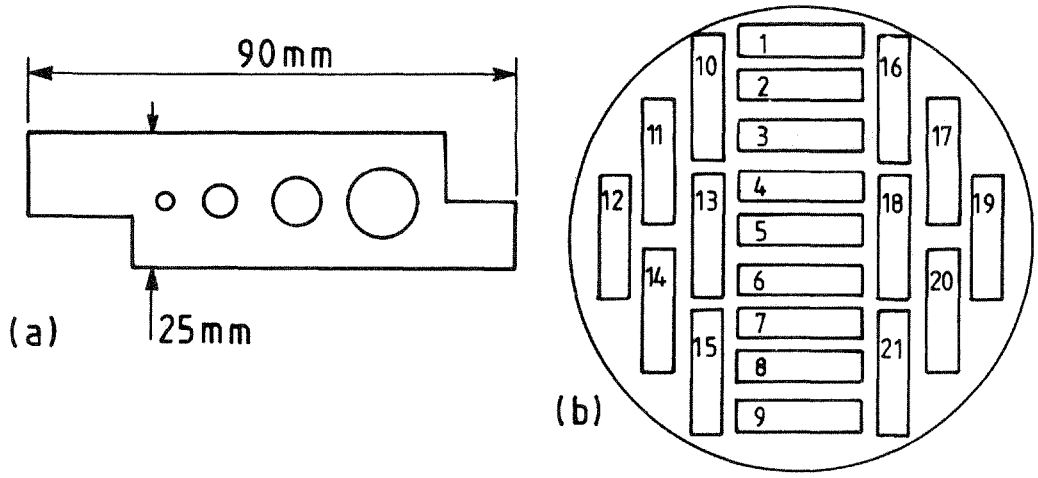

Figure 4. Part geometry (a) and layout (b).

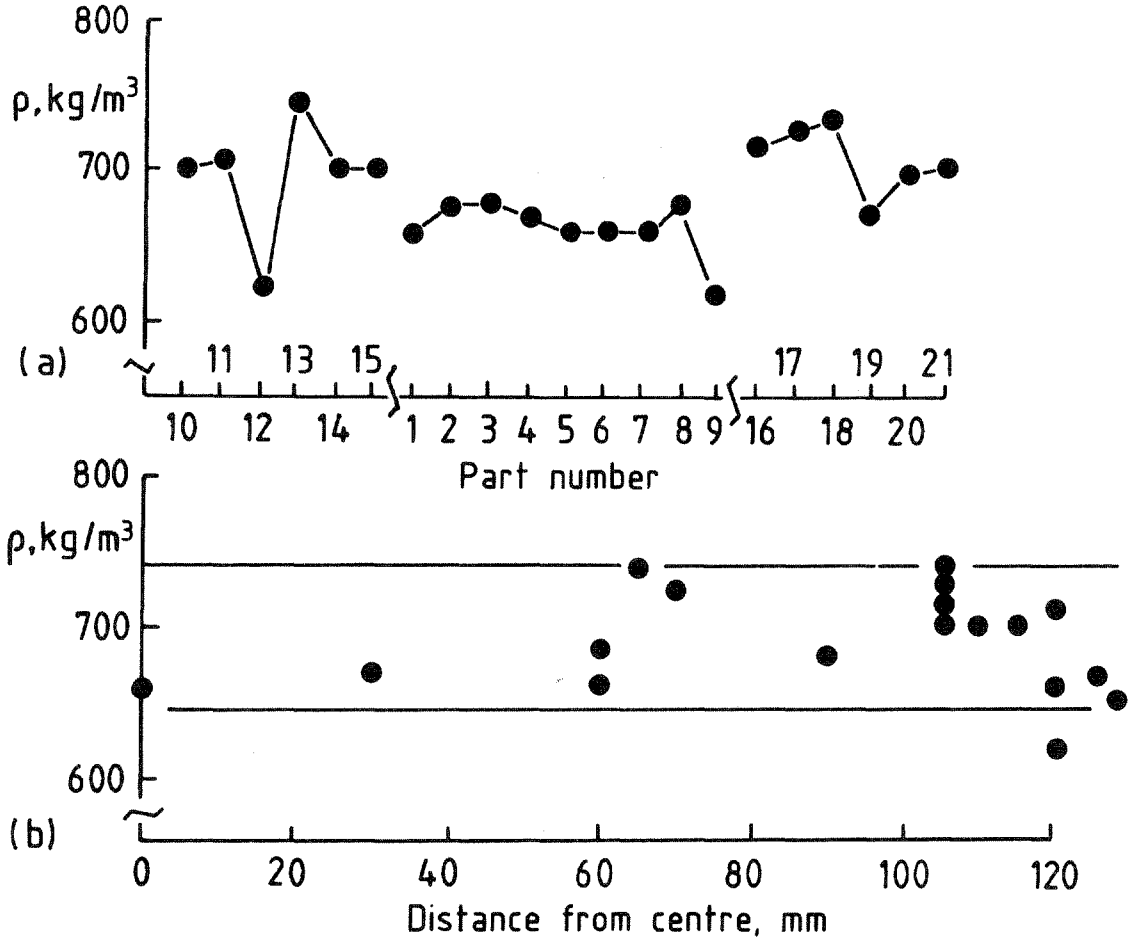

Figure 5. Density variations in nominally constant conditions arranged (a) by part number and (b) by distance from the centre of the build area.

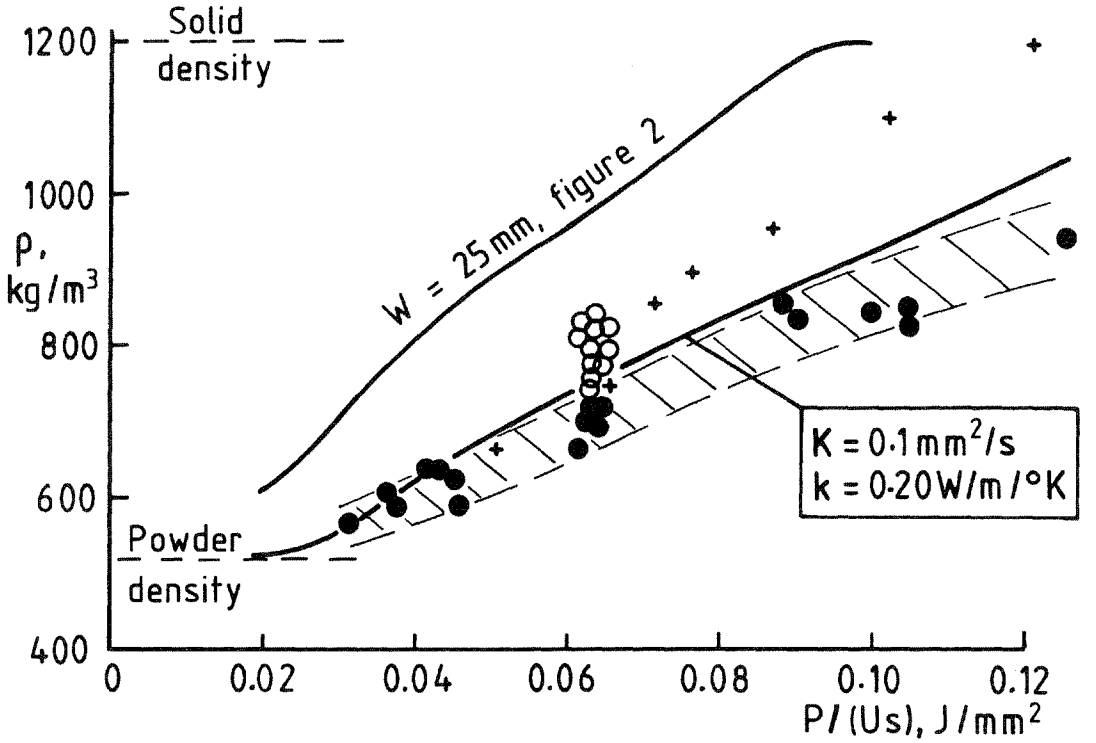

Figure 6. Predicted (—) and experimental (•, o, +) density variations.

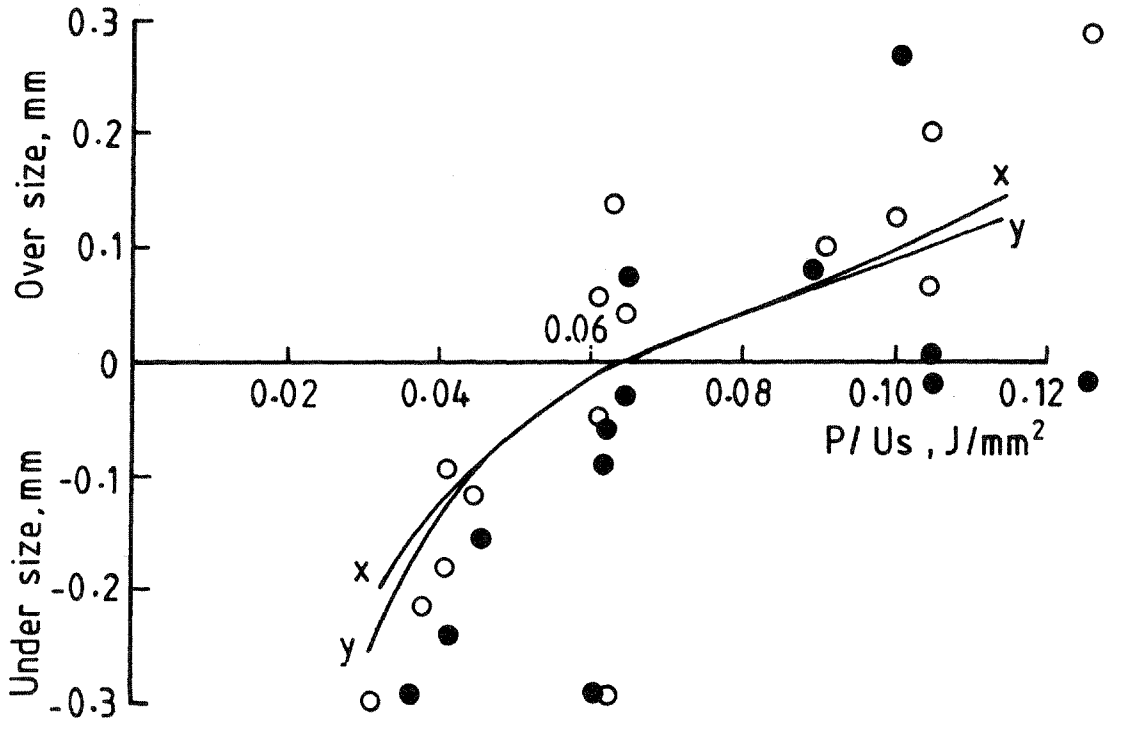

Figure 7. Predicted (—) and experimental x (•) and y (o) out of size, shifted to coincide at P/(Us) = 0.063 J/mm^2.